Available online at www.sciencedirect.com

ScienceDirect

IFAC Papers Online CONFERENCE PAPER ARCHIVE

IFAC PapersOnLine 50-1 (2017) 10413–10418

Double Loop Control Design for Boost Converters Based on Frequency Response Data ⋆

Ricardo Alzate ** **Vilma A. Oliveira** * **Rafael F. Q. Magossi** *
Shankar P. Bhattacharyya ***

* *Department of Electrical and Computing Engineering, Universidade de São Paulo, São Carlos, SP, Brazil (e-mail:vilma@sc.usp.br)*
** *School of Electrical Engineering, Universidad Industrial de Santander, Bucaramanga, Colombia (e-mail: ralzatec@uis.edu.co)*
*** *Department of Electrical and Computer Engineering, Texas A&M University, College Station, USA (e-mail: bhatt@ece.tamu.edu)*

Abstract: This paper presents a data driven approach for PI control design based on frequency response data and calculations of stabilizing sets. The geometrical interpretation of the loci of stability margins allows to determine the parameters of a PI controller from a space of achievable specifications, constructed from frequency response data. As illustration for the use of the proposed approach in engineering applications, regulation of the output voltage of a boost power converter circuit under a double loop control strategy is presented. Numerically, it was possible to generate enough amount of data to perform accurate predictions. The key to apply the proposed approach with success was the generation of a Bode diagram for the system with fine resolution, avoiding the explicit necessity for mathematical models.

Keywords: Boost converter, data driven, frequency response, PI control, stabilizing sets.

1. INTRODUCTION

There are two main approaches to perform control synthesis tasks. The first approach is model-based control and the control parameters are calculated using a model of the plant. Depending on the complexity of the system under study, finding a model can be cumbersome. A second approach is to extract information of the system behavior directly from data. This approach is known as data-driven and are generally model-free. The latter is an approach more suited to deal with uncertainties and unexpected changes in the structure of the system.

In relation to the case of fixed order controllers, the set of stabilizing controllers of PI and PID type can be determined based on frequency response data of the plant (Keel and Bhattacharyya, 2008). Characterization of all stabilizing fixed order controllers is critical for designing controllers which satisfy performance specifications which are based on frequency response, such as gain and phase margins (Alzate and Oliveira, 2016). This constitutes a modern approach to PI and PID control design, representing an alternative to traditional methods in general of the trial and error type.

Power converter circuits are strategic devices in energy management as they regulate power flows from sources to loads. They can be modeled as small-signal transfer functions when operating close to an operating point, allowing the use of traditional techniques for analysis and synthesis (Chen et al., 2011; Wai and Shih, 2011). One of the most popular types of power converters used in applications is the boost topology, in which the output voltage is higher than the one provided as input. However, despite its popularity, this circuit presents a structural drawback related to a non-minimum phase behavior whenever the voltage is selected as the system output, representing a challenge from the control viewpoint (Hoagg and Bernstein, 2007). Special effort has been devoted to understand and compensate the non-minimum phase feature of the boost topology under voltage mode (Bag et al., 2013). Recent developments as those reported in Lopez-Santos et al. (2015) calculate parameters for low-order controllers of power converters attending specifications with respect to stability margins.

In this paper, we explore a novel approach to design PI controllers which employs a geometrical approach to relate stabilizing controllers with a space of achievable specifications computed from frequency response data. The approach is model free and provides information about the system performance based on analytical formulations.

2. STABILIZING SETS

Let us consider the LTI plant

$$P(s) = \frac{N(s)}{D(s)} \tag{1}$$

in cascade with a PI controller

⋆ This work was supported by the Brazilian National Council for Scientific and Technological Development (CNPq) under Ciência Sem Fronteiras Program grant 400401/2013-4, 150228/2015-5 and 150339/2016-0.

10.1016/j.ifacol.2017.08.1968

$$C(s) = \frac{k_p s + k_i}{s} \tag{2}$$

such that

$$\delta(k_i, k_p, s) = sD(s) + (k_p s + k_i)\, N(s) \tag{3}$$

represents the characteristic polynomial for an unity feedback system. The stabilizing set contains all PI controllers that stabilize the closed loop for the plant $P(s)$ and is given by

$$\mathcal{S} := \{(k_i, k_p) : \delta\,(s, k_i, k_p) \text{ is Hurwitz}\}\,. \tag{4}$$

2.1 Stability From the Signature of a Rational Function

Let us now define the following rational functions based on $\delta(k_i, k_p, s)$

$$\begin{aligned} F(s) &:= \frac{\delta(k_i, k_p, s)}{D(s)} = s + (k_p s + k_i)P(s) \\ \bar{F} &:= F(s)P(-s). \end{aligned} \tag{5}$$

The location of zeros and poles of $F(s)$ (excluding roots on the $j\omega$ axis) can be related to its net change in phase as ω varies from 0 to $+\infty$, expressed by

$$\Delta_0^{\infty} \angle F(j\omega) = \frac{\pi}{2}\sigma(F) \tag{6}$$

with $\sigma(F)$ representing the signature of $F(s)$.
The signature $\sigma(F)$ can be defined in terms of the number of zeros z_F and poles p_F of $F(s)$ located in the left (-) and right (+) half sides of the complex plane, as follows Keel and Bhattacharyya (2008)

$$\sigma(F) := \left(z_F^- - z_F^+\right) - \left(p_F^- - p_F^+\right). \tag{7}$$

The closed loop system is stable if all its characteristic roots are in the left half of the complex plane, then for stability we need $z_F^+ = 0$.

If the relative degree of $P(s)$ is $r_P = (n-m)$ for $n > m$, the degree of $\delta(s)$ is $(n+1)$ and then $z_F^- = (n+1)$. Accordingly

$$\sigma(F) = (n+1) - \left(p_F^- - p_F^+\right). \tag{8}$$

By extending the signature concept to $P(s)$ we get

$$\sigma(P) = (z_P^- - z_P^+) - (p_P^- - p_P^+)$$

and equivalently

$$\sigma(P(-s)) = \left(z_P^+ - z_P^-\right) - \left(p_P^+ - p_P^-\right). \tag{9}$$

Then

$$\sigma(\bar{F}) = \sigma(F(s)) + \sigma(P(-s) = (n+1) + (z_P^+ - z_P^-). \tag{10}$$

Now, since $z_P^+ + z_P^- = m$ it is possible to write

$$z_P^+ - z_P^- = 2z_P^+ - m \tag{11}$$

so that the signature for closed loop stability of $P(s)$ under PI control is

$$\sigma(\bar{F}) = (n+1) + (2z_P^+ - m) = n - m + 2z_P^+ + 1. \tag{12}$$

2.2 Numerical Computation of the PI Stabilizing Set

In order to analyze the effect of the PI control parameters on the poles and zeros of $F(s)$, it is convenient to separate the dependence of the real and imaginary parts of $F(j\omega)$ on k_p and k_i.
This can be achieved after multiplying $F(j\omega)$ by $P(-j\omega)$, with

$$P(j\omega) = P_r(\omega) + jP_i(j\omega) \tag{13}$$

representing the frequency response of the plant, allowing to get

$$\begin{aligned} \bar{F}(j\omega) &= F(j\omega)P(-j\omega) \\ &= \bar{F}_r(\omega, k_i) + j\omega\bar{F}_i(\omega, k_p) \end{aligned} \tag{14}$$

for

$$\bar{F}_r(\omega, k_i) := \omega P_i(j\omega) + k_i|P(j\omega)|^2 \tag{15}$$

$$\bar{F}_i(\omega, k_p) := P_r(\omega) + k_p|P(j\omega)|^2. \tag{16}$$

Now, fix $k_p = k_p^*$ and set

$$\bar{F}_i(\omega, k_p^*) = 0 \tag{17}$$

which is equivalent to

$$k_p^* = -\frac{P_r(\omega)}{|P(j\omega)|^2} =: g(\omega) \tag{18}$$

The zeros of (17) are the ω values

$$0 < \omega_1 < \omega_2 < \cdots < \omega_{l-1} < \infty^- \tag{19}$$

satisfying (18).

The signature in (12) can be alternatively expressed by (Keel and Bhattacharyya, 2008)

$$\begin{aligned} \sigma(\bar{F}) = [&i_0 - 2i_1 + 2i_2 + \cdots + \\ &+ (-1)^{l-1}2i_{l-1} + (-1)^l \Lambda i_l]\Gamma, \end{aligned} \tag{20}$$

where

$$\Lambda = \begin{cases} 1, \text{ if } r_{\bar{F}} \text{ is even} \\ 0, \text{ if } r_{\bar{F}} \text{ is odd} \end{cases} \tag{21}$$

$$\Gamma = (-1)^{l-1}\,\mathrm{sgn}(\bar{F}_i(\omega_l, k_p^*)) \tag{22}$$

$$i_k = \mathrm{sgn}\left(\bar{F}_r\,(\omega_k, k_i)\right), \tag{23}$$

with sgn(.) as the signum function and

$$\begin{aligned} r_{\bar{F}} &= r_F + r_P \\ &= n - m + 1 \end{aligned} \tag{24}$$

being the relative degree of $\bar{F}$ and for $\omega_k, k = \{0, 1, 2, \cdots, l\}$ as in (19) with $\omega_0 = 0$ and $\omega_l = \infty^-$.

Hence, whenever the following inequality holds

$$2l - 1 + \Lambda \geq n - m + 2z_P^+ + 1 \tag{25}$$

it is possible to find combination of patterns for $i_k \in \{-1, 1\}$ achieving the signature requirement (12). These patterns allow us to solve from (23), the corresponding k_i values satisfying stability. These specifies the range over which k_p must be swept. By sweeping over k_p values and repeating the procedure we can generate numerically the stabilizing set $\mathcal{S}$ in (6).

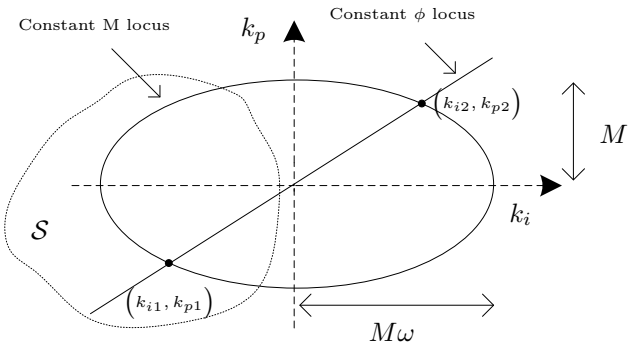

Fig. 1. Constant M and ϕ loci for PI controllers.

2.3 Stability Margins in the PI plane

Consider the frequency response for the PI controller in (2). Then, by defining

$$M = |C(j\omega)|, \phi = \angle C(j\omega)$$

we can write

$$\frac{k_p^2}{M^2} + \frac{k_i^2}{M^2\omega^2} = 1, \quad -\omega\tan(\phi)k_p = k_i \tag{26}$$

which represents an ellipse (with radii M in the k_p axis and $M\omega$ in the k_i axis) and a straight line in the (k_i, k_p) plane, as shown in Fig. 1.

The geometrical representation of the controllers can be employed for calculation of parameters of a PI controller attaining specifications in frequency domain, following the procedure given below:

1. If the closed loop of the system is stable, there is a phase margin θ_m defined by
$$\theta_m := \angle P(j\omega_g) + \angle C(j\omega_g) - \pi,$$
in terms of the gain crossover frequency ω_g satisfying
$$|P(j\omega_g)||C(j\omega_g)| = 1;$$
2. If $P(j\omega)$ is known, fixing $\omega = \omega_g$ defines the following ellipse in the (k_i, k_p) space
$$\frac{k_p^2}{M^2} + \frac{k_i^2}{M^2\omega_g^2} = 1, \; M = |P(j\omega_g)|^{-1} \tag{27}$$
3. If we now require a phase margin θ_m, we must have the angle condition
$$\phi = \theta_m + \pi - \angle P(j\omega_g)$$
represented in the (k_i, k_p) space by the straight line
$$-\omega_g\tan(\phi)k_p = k_i; \tag{28}$$
4. The points in the (k_i, k_p) plane satisfying simultaneously (27) and (28) are those attaining the required phase margin θ_m and gain crossover frequency ω_g, provided they lie in the stabilizing set. This is the case for (k_{i1}, k_{p1}) in Fig. 1.

2.4 Space of Achievable Specifications

The set of achievable (ω_g, θ_m) points in the specifications domain, can be generated from $\mathcal{S}$ in a surjective manner, that is, each point in the achievable performance set can be attained by at least one stabilizing controller by using computational tools, as follows:

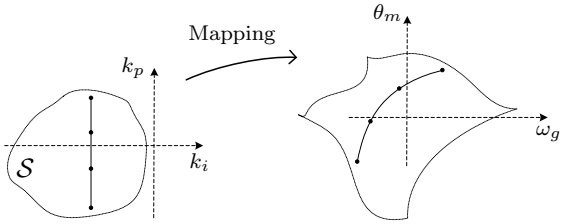

Fig. 2. Space of achievable design specifications generated from points of the stabilizing set $\mathcal{S}$.

1. Fix k_i and let $\left[k_p^-, k_p^+\right]$ denote the range of k_p within the stabilizing set $\mathcal{S}$, to be explored;
2. By choosing controllers along this line, we obtain a curve in the design space, which is a set of points (ω_g, θ_m), as depicted in Fig. 2;
3. The entire set $\mathcal{S}$, can be scanned by letting k_i range over the stabilizing values and repeating.

3. VOLTAGE REGULATION OF A BOOST CONVERTER

A DC-DC boost power converter circuit is a device of wide use in power stages of modern electric and electronic equipment as a coupling interface between sources and loads. The converter is employed as an element for energy management (Rashid, 2011).

The average-model for the dynamics of a boost type power converter, under continuous-conduction-mode (CCM) and ideal devices, can be stated as follows (Wai and Shih, 2011):

$$\frac{di}{dt} = -\frac{(1-u)}{L}v + \frac{E}{L}; \quad \frac{dv}{dt} = \frac{(1-u)}{C}i - \frac{v}{RC} \tag{29}$$

where i represents the average inductor current, v the average output (capacitor voltage) and $u \in (0, 1)$ is the average control, parameters R, L, C are resistance, inductance and capacitance, respectively, and E is the supply voltage of the circuit.

Define the state variables as the magnitudes at the energy storing elements, that is, $\mathbf{x} = [\, i \;\; v \,]^T$, then (29) describes an affine system with respect to the input $u(t)$.

The non-minimum phase behavior of boost power converters has been the subject of several articles reported in the literature. See for instance Bag et al. (2013). As a way to overcome this undesired behavior, a multivariate approach known as current-mode control Alvarez-Ramirez et al. (2001) allows to perform indirect regulation of voltage through a double-loop scheme, where the inductor current is controlled by a reference signal depending on the capacitor voltage.

According to Utkin et al. (1999), boost converters satisfy the *motion separation principle*, meaning that the motion rate of the current is much faster than the motion rate of the output voltage. Then the control problem (indirect voltage regulation) can be solved by the interaction of an inner current control loop with an outer voltage control loop. From the many ways proposed to solve the indirect regulation, in this paper we adopted a cascade PI sliding-mode control (SMC) approach, as depicted in Fig. 3.

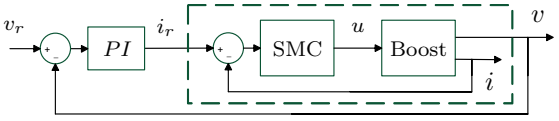

Fig. 3. Double-loop indirect voltage regulation scheme.

3.1 Inner Current Loop

The current loop is based on a high-frequency switching strategy, calculated by the SMC signal Utkin et al. (1999)

$$u = \frac{1}{2}\left(1 - \operatorname{sgn}(S)\right) \tag{30}$$

where $S = i - i_r$ representing the sliding surface with

$$i_r = \frac{V^2}{RE} \tag{31}$$

defining the desired inductor current in terms of the steady-state value V for the output voltage v. The existence of the sliding-mode in the vicinity of $S = 0$ is guaranteed after accomplishment of the sliding condition

$$S\frac{dS}{dt} < 0 \text{ with } \frac{dS}{dt} = \frac{di}{dt} = -\frac{(1-u)}{L}v + \frac{E}{L}. \tag{32}$$

Expression (32) is satisfied for $v > E$, implying the existence of the sliding mode as long as the output voltage is higher than the source voltage. This constraint is easily verified for a boost converter topology. selected.

3.2 Outer Voltage Loop

The voltage loop can be handled easily with a PI control action. This implies a representation equivalent to an unity feedback system for the outer loop and a small-signal (linear) model for the inner current loop as the system plant $P(s)$. The transfer function relating v and i_r in Fig. 3, can be generated analytically as presented by Chen et al. (2011).

However, as can be noticed from results presented in Section 2, the proposed method for calculation of the PI control parameters requires only the knowledge of the frequency response $P(j\omega)$ for the plant and we do not need an explicit knowledge for the transfer function $P(s)$.

This appears as an advantage for practical applications where it is too cumbersome to identify the plant. Then, calculations for $P(j\omega)$ can be easily performed experimentally as will be shown later, constituting the base for the data driven design approach proposed in this paper.

4. PI CONTROL DESIGN FOR THE VOLTAGE LOOP

In order to analyze numerically the behavior of the double-loop structure proposed in Fig. 3, the same schematic diagram depicted described in Alzate and Oliveira (2016) is used. The simulation scenario includes variation in the supply voltage (denoted δE) and a step change in the voltage reference v_r.

4.1 Inner Current Loop Analysis

To apply the PI design approach proposed, it is of fundamental importance to assure that the inner current loop is operating under small-signal regime, validating the representation for the outer voltage loop depicted in Fig. 3. A simple way to verify this is by constructing its frequency response (Bode diagram). To this aim, the *AC Sweep* analysis tool of PSIM was configured to apply a sinusoidal variation on the reference of the current loop (isolating the voltage loop) with amplitude of 10 % its nominal value (31).

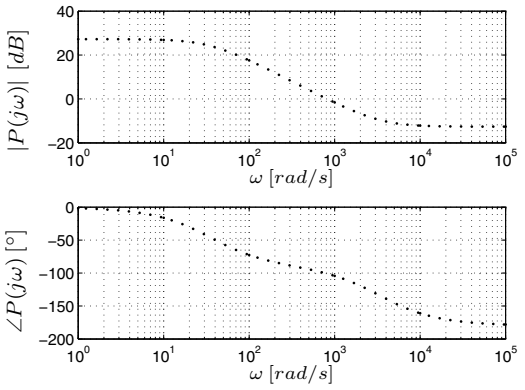

Fig. 4. Bode diagram for the inner current loop calculated from *AC Sweep* analysis in PSIM.

As a result, Fig. 4 depicts the curves for magnitude and phase obtained by using 46 points of frequency within the interval [0.1, 15000] Hz. For validation purposes, the agreement between these results and the analytical model proposed by Chen et al. (2011) was verified, confirming the appropriate operation of the current loop under SMC.

4.2 PI Stabilizing Set for the Voltage Loop

The relative degree $(n - m)$ of the plant can be inferred from the high frequency slope of the magnitude plot in Fig. 4. The Bode diagram shows $0\,dB/decade$ suggesting $(n - m) = 0$. In terms of the phase response, the Bode diagram depicts a net change in phase $\Delta_0^\infty \angle P(j\omega) = -\pi$, such that from (6) we can write

$$\begin{aligned}\Delta_0^\infty \angle P(j\omega) &= \frac{\pi}{2}\left[\left(z_P^- - z_P^+\right) - \left(p_P^- - p_P^+\right)\right] \\ &= \frac{\pi}{2}\left[\left(z_P^- + z_P^+ - 2z_P^+\right) - \left(p_P^- + p_P^+ - 2p_P^+\right)\right] \\ &= -\pi\end{aligned}$$

which yields $z_P^+ - p_P^+ = 1$.

Given that the plant is stable we have $p_P^+ = 0$ and then $z_P^+ = 1$, confirming the non-minimum phase feature of the boost converter. From (12) we have

$$\sigma(\bar{F}) = n - m + 2z_P^+ + 1 = 3$$

In Fig. 5 the function $g(\omega)$ is depicted, showing a one-to-one mapping from ω to k_p^* values, or equivalently, for $(l - 1) = 1$. Hence

$$\omega_k = \{\omega_0,\, \omega_1,\, \omega_2\} = \{0,\, \omega_1,\, \infty^-\}$$

with ω_1 representing the inverse mapping through $g(\omega)$ for a k_p^* value selected in the interval $[-0.0435, 4.2689]$. Now,

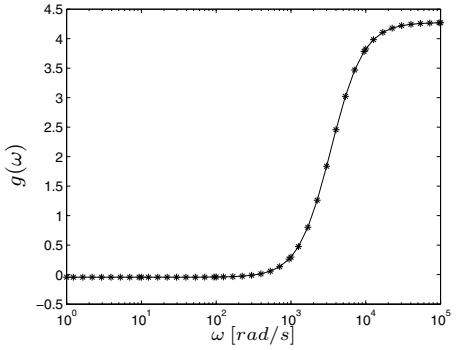

Fig. 5. Function $g(\omega)$ mapping ω into k_p values.

by recalling (24) we have

$$r_{\bar{F}} = n - m + 1 = 1$$

such that $\Lambda = 0$ in (21). This accomplishes the condition imposed by (25) as follows

$$2l - 1 + \Lambda \geq 3$$
$$l \geq \frac{3 + 1 - \Lambda}{2} = 2$$

giving the combination patterns for i_k satisfying (20). Also, by noticing that

$$\bar{F}_i(\omega_l, k_p^*) = k_p^* - g(\omega_l)$$

it is clear from Fig. 5 that $\bar{F}_i(\infty^-, k_p^*) < 0$ and then $\Gamma = +1$ in (22). Thus, (20) takes the form

$$\sigma(\bar{F}) = i_0 - 2i_1 = 3$$

such that the only pattern achieving the signature condition is $\{i_0, i_1\} = \{1, -1\}$.

From (23) we get

$$1 = \text{sgn}(\bar{F}_r(\omega_0, k_i)), \quad -1 = \text{sgn}(\bar{F}_r(\omega_1, k_i))$$

implying

$$\bar{F}_r(\omega_0, k_i) > 0, \ k_i|P(j\omega_0)|^2 > 0 \quad k_i > 0, \tag{33}$$

and

$$\bar{F}_r(\omega_1, k_i) < 0, \quad \omega_1 P_i(\omega_1) + k_i|P(j\omega_1)|^2 < 0$$
$$k_i < \frac{-\omega_1 P_i(\omega_1)}{|P(j\omega_1)|^2}. \tag{34}$$

Finally, Fig. 6 depicts the stabilizing set $\mathcal{S}$ calculated by solving numerically the pair (k_p, k_i) of values satisfying

$$0 < k_i < \frac{-\omega_1 P_i(\omega_1)}{|P(j\omega_1)|^2},$$

for $\omega_1 = g^{-1}(k_p^*)$ with $k_p^* \in [-0.0435, 4.2689]$.

4.3 Practical Constraints on the Stabilizing Set

The method just described for calculation of the stabilizing set was formulated without explicit consideration about practical restrictions on the operation of the system. Taking into account the saturation limits imposed to

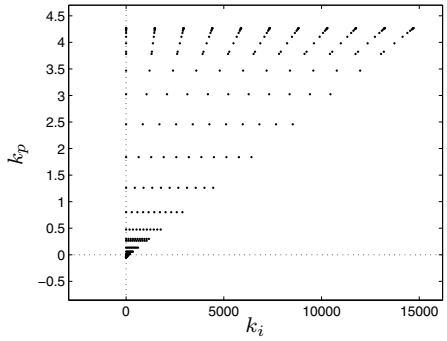

Fig. 6. PI Stabilizing set $\mathcal{S}$ calculated from measurement data.

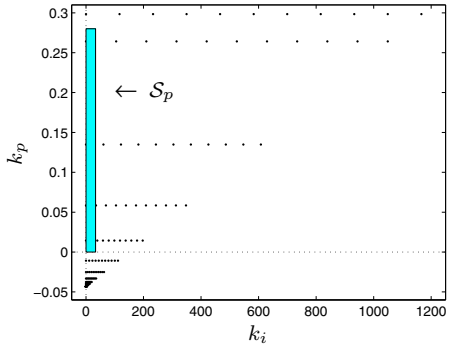

Fig. 7. Practical PI stabilizing set $\mathcal{S}_p$ after constraining the signals of the voltage loop.

signals on the double-loop circuit, it is important to verify practical boundaries for the stabilizing set. To this aim, simulations were performed in PSIM.

Then, a proportional (only) controller was tested to determine the loop gain $k_p = 0.28$ achieving the maximum current (3 $[A]$) allowed in practice. In a similar manner, an integral controller determined $k_i = 33.33$ as the gain reaching saturation limits in current for the closed loop. Hence, a subset $\mathcal{S}_p$ of $\mathcal{S}$ defined as follows

$$\mathcal{S}_p := \{(k_i, k_p) : k_i \in [0,\ 33.33], k_p \in [0,\ 0.28]\} \tag{35}$$

is a practical PI stabilizing set which incorporates constraints on the signals of the voltage loop.

Lower boundaries of the subset have been selected arbitrarily inside of the stable region suggested *a priori* by $\mathcal{S}$. Figure 7 depicts the corresponding subset $\mathcal{S}_p$, illustrating the reduced amount of achievable values with respect to $\mathcal{S}$ imposed by practical constraints.

4.4 Practical Achievable Specifications

Following the procedure proposed in Section 2.4, the set of achievable (ω_g, θ_m) points in the specifications domain, can be generated from $\mathcal{S}_p$ by sweeping the range of admissible (k_i, k_p) values and mapping the corresponding image for each point in terms of equivalent design requirements.

Results for the set of practical achievable specifications in the (ω_g, θ_m) space are depicted in Fig. 8, from which four testing points have been selected as samples of achievable scenarios, covering the intervals: $25° \leq \theta_m \leq 95°$; 60 rad/s $\leq \omega_g \leq$ 160 rad/s. The sample points can be

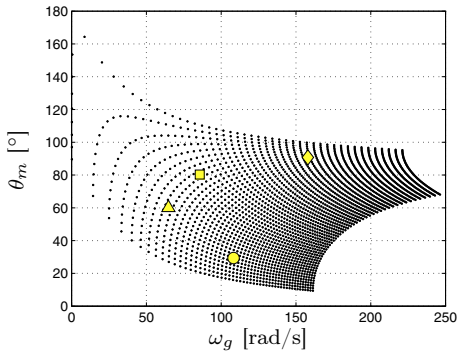

Fig. 8. Design parameter plane for the voltage regulation loop under PI control relating the phase margin θ_m and its corresponding gain crossover frequency ω_g.

mapped back to the (k_i, k_p) plane by applying the procedure based on ellipses and straight lines described in Section 2.3, producing the results depicted in Fig. 9 for controllers attaining the required specifications.

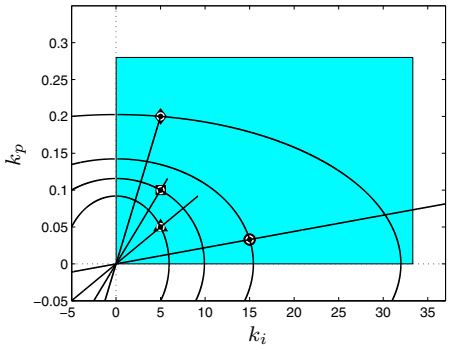

Fig. 9. Points of the practical stabilizing set $\mathcal{S}_p$ (35) depicted as intersections of constant M and ϕ loci for PI controllers.

As the design has been formulated in terms of requirements in frequency domain, a verification of time domain features is required and performed by a step response on the four controllers analyzed. Figure 10 shows the time responses for the output voltage v under the simulation scenario proposed, depicting several qualitative features for the different cases considered such as reference changes from 80 to 85 $[V]$ at $t = 0.3$ $[s]$ and disturbances in the supply voltage E varied from 30 to 25 $[V]$ at $t = 0.7$ $[s]$.

5. CONCLUDING REMARKS

A PI control design based on frequency response data was formulated and applied numerically to regulate the output voltage of a double-loop configuration of a boost power converter circuit. The proposed design methodology employed the stability conditions for LTI systems provided by the signature of a rational function and the corresponding calculation of stabilizing sets based on its frequency response. This was combined with a geometrical interpretation for the phase margin θ_m and the gain crossover frequency ω_g of PI control loops in terms of ellipses and straight lines in the (k_i, k_p) plane to generate the space of specifications achievable in practice.

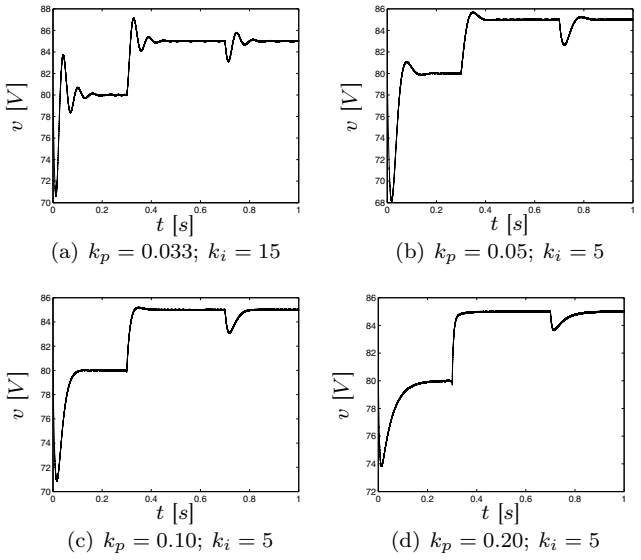

(a) $k_p = 0.033$; $k_i = 15$ (b) $k_p = 0.05$; $k_i = 5$

(c) $k_p = 0.10$; $k_i = 5$ (d) $k_p = 0.20$; $k_i = 5$

Fig. 10. PSIM simulations of output v under PI controllers.

REFERENCES

Alvarez-Ramirez, J., Cervantes, I., Espinosa-Perez, G., Maya, P., and Morales, A. (2001). A stable design of PI control for DC-DC converters with an RHS zero. *IEEE Transactions on Circuits and Systems I: Fundamental Theory and Applications*, 48(1), 103–106.

Alzate, R. and Oliveira, V.A. (2016). Multiobjective design of PI controllers with applications. In *2016 IEEE Conference on Control Applications*, 203–214.

Bag, S., Roy, T., Mukhopadhyay, S., Samanta, S., and Sheehan, R. (2013). Boost converter control using Smith predictor technique to minimize the effect of right half plane zero. In *2013 IEEE International Conference on Control Applications*, 983–988.

Chen, Z., Gao, W., Hu, J., and Ye, X. (2011). Closed-loop analysis and cascade control of a nonminimum phase boost converter. *IEEE Transactions on Power Electronics*, 26(4), 1237–1252.

Hoagg, J.B. and Bernstein, D.S. (2007). Nonminimum-phase zeros - much to do about nothing - classical control - revisited part II. *IEEE Control Systems*, 27(3), 45–57.

Keel, L. and Bhattacharyya, S. (2008). Controller synthesis free of analytical models: Three term controllers. *IEEE Transactions on Automatic Control*, 53(6), 1353–1369.

Lopez-Santos, O., Martinez-Salamero, L., Garcia, G., Valderrama-Blavi, H., and Sierra-Polanco, T. (2015). Robust sliding-mode control design for a voltage regulated quadratic boost converter. *IEEE Transactions on Power Electronics*, 30(4), 2313–2327.

Rashid, M.H. (2011). *Power Electronics Handbook: Devices, Circuits and Applications*. Butterworth-Heinemann, 3 edition.

Utkin, V., Guldner, J., and Shi, J. (1999). *Sliding Mode Control in Electromechanical Systems*. Taylor & Francis.

Wai, R. and Shih, L. (2011). Design of voltage tracking control for DC-DC boost converter via total sliding-mode technique. *IEEE Transactions on Industrial Electronics*, 58(6), 2502–2511.